Journal of Sound and Vibration (2002) **251**(4), 631–649
doi:10.1006/jsvi.2001.3734, available online at http://www.idealibrary.com on IDEAL®

ANALYSIS AND MEASUREMENT OF SOUND TRANSMISSION THROUGH A DOUBLE-WALLED CYLINDRICAL SHELL

J.-H. Lee and J. Kim

Structural Dynamics Research Laboratory, Mechanical Engineering Department, University of Cincinnati, Cincinnati, OH 45221-0072, *U.S.A. E-mail: jay.kim@uc.edu*

(*Received* 14 *January* 2000, *and in final form* 3 *April* 2001)

Sound transmission through a double-walled cylindrical shell is studied. The solution that describes the system response is obtained by combining the solutions of two different models of the system. The first model, which describes the sound transmission due to the interaction between the acoustic waves and the bending waves in the shells, is formulated by three acoustic wave equations and two shell vibration equations. The second model describes the sound transmission by one-dimensional waves propagating through the layers of the shells and the air-gap. The transmission losses calculated from the two models are combined to represent the system response in the entire frequency range. Analytical solutions are compared to corresponding measured results, which shows reasonable agreements if the extent of the simplifications used in the analytical model is considered. The effects of important design parameters such as the air-gap size and the thickness ratio are studied using analytical solutions.

1. INTRODUCTION

Double-walled flat or curved panels are found in many applications because they are effective sound barriers that can increase the transmission loss (TL) over the equivalent single-wall construction. Problems of sound transmission through panels of single or double walls and sandwich panels have been investigated by many researchers, which are mostly analytical efforts [1–12]. White [12] compared the analytical result with the experimental measurement for a finite cylindrical single-walled shell for very limited cases. In the authors' previous work [13], the sound transmission through a single-wall cylindrical shell was studied. In the work, an exact solution was obtained in a series form using a classical shell vibration equation without ignoring any of the three directions of shell motions.

The desire to obtain design rules of thin, double-wall shells used as the side surface of high-end automotive mufflers served as the practical motivation for this work. In such applications, two thin plates are combined by spot welding, and rolled into a circular or elliptical cylinder shape. Some simplifications of the problem are made so that it can be solved exactly. First, the length of the system is assumed to be infinite, which eliminates the need to consider the effect of the boundary conditions at the end of the shell. Second, the incident acoustic wave is assumed to be a plane wave. Finally, an anechoic condition is assumed in the interior cavity. The first and second simplifications reduce the problem is consideration to a two-dimensional (2-D) problem, as it will be explained. The second and

0022-460X/02/140631 + 19 $35.00/0

third idealizations make the model a rough reciprocal of a muffler tested in an anechoic chamber, which has an anechoic condition outside and a diffusive field inside.

Two different system models are combined to obtain the transmission loss (TL) of the system. The first model is used to calculate the sound transmission due to the transverse bending waves in the shells and the acoustic waves. In this model, the system equation is composed of two sets of shell vibration equations and three acoustic wave equations for the external, gap and internal spaces. The exact solution to these equations is obtained in series forms, and represented in terms of TL. The second model is used to calculate the sound transmission caused by the compression/rarefaction waves in the shell and the acoustic space, in which the shells are treated like fluid. The model is described by a one-dimensional (1-D) wave propagating through three layers of acoustic media, two shell layers and one air-gap layer. It is found that the TL from the 1-D model is lower than the TL from the 2-D model in the low-frequency range, and vice versa in the high-frequency range. Considering the definition of the TL (lower TL means higher transmitted sound), it is easily realized that the lower TL curve should be taken to represent the system response. Therefore, the system TL is obtained by combining TL curves from the 1-D and 2-D models. This superposition concept is introduced for the first time in this work.

Sound transmissions through single and double shells are measured experimentally, to which the theoretical solutions are compared. Single- and double-walled shells used in the experiment had the same dimensions and properties as the theoretical model except their finite lengths. Thick end caps were used to close both ends of the cylinders to eliminate the effect of the sound radiated from the end plates. TLs are measured in an anechoic chamber, once with the sound source located inside the cylinder and the other time with the sound source located outside the cylinder. If the reciprocity is considered, it is realized that these set-ups are rough equivalents to each other. The main purpose of the experimental comparison is to confirm that the formulation and computation procedure of the problem are free of fundamental errors, which is always a possibility in a numerical model without experimental validation. Utilizing the advantage of having a theoretical procedure validated experimentally, the effect of important parameters such as thickness ratio and the size of the air-gap are studied.

2. ANALYTICAL SOLUTION PROCEDURE

2.1. SOUND TRANSMISSION BY BENDING WAVES IN SHELLS

Figure 1 shows a schematic of two concentric cylindrical shells of infinite length. R_i, R_e, h_i and h_e indicate the radii and thickness of the shells, in which the subscripts i and e represent the inner and outer shells in general. As shown in the figure, a plane wave is incident with an angle γ and reflected by the external surface of the cylinder. Only the transmitted wave is considered in the internal cavity. The reflected waves are ignored in the internal cavity to make the model approximate the reciprocal of a muffler tested in an anechoic chamber, which has the incident and reflected waves internally and only transmitted waves externally.

2.1.1. *Formulation of the governing equations*

The fluid media in the external, in-between, and the internal space are defined by the density and the speed of sound: $\{\rho_1, c_1\}$, $\{\rho_2, c_2\}$ and $\{\rho_3, c_3\}$ respectively. Properties of the shells are defined by the density, Young's modulus, and the Poisson ratio: $\{\rho_i, E_i, \mu_i\}$, $\{\rho_e, E_e, \mu_e\}$. The incoming noise is idealized as a plane wave p^I travelling in the x–z plane incident with an angle γ_1 as shown in the figure.

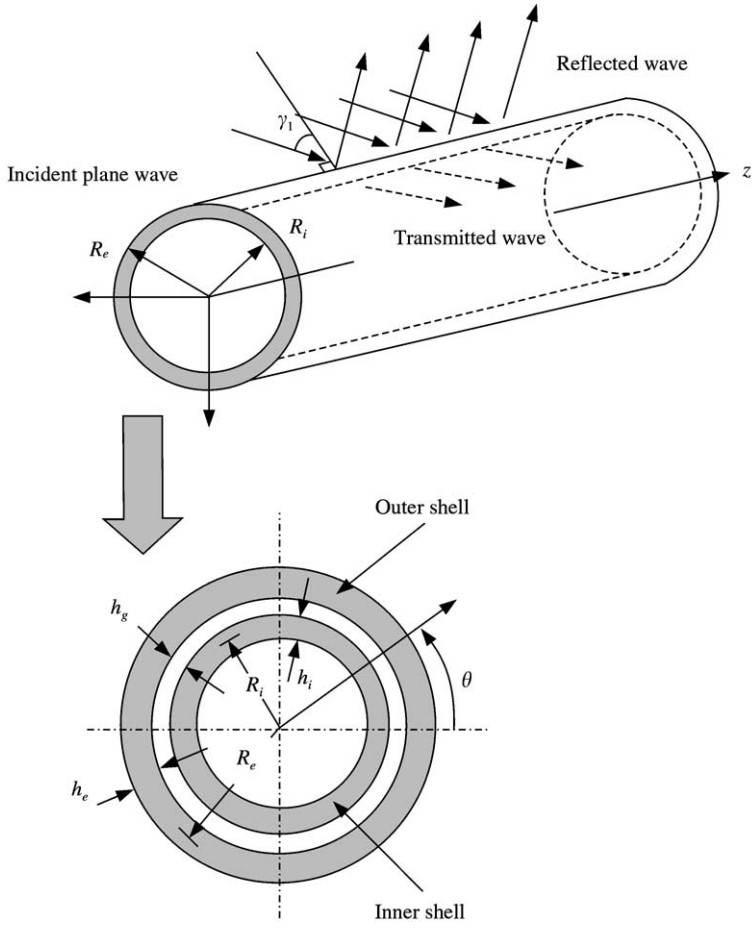

Figure 1. Schematic description of the problem: 2-D model.

The acoustic pressure in the external space $p_1 = p^I + p_1^R$, where p^I is the incident wave and p_1^R is the reflected wave, satisfies the wave equation [14]

$$c_1 \nabla^2 (p^I + p_1^R) + \frac{\partial^2 (p^I + p_1^R)}{\partial t^2} = 0, \tag{1}$$

where ∇^2 is the Laplacian operator. In the annular space between the shells, the pressure is $p_2 = p_2^T + p_2^R$, where p_2^T is the transmitted wave through the external shell and p_2^R is the reflected wave from the internal shell, which satisfies the acoustic wave equation

$$c_2 \nabla^2 (p_2^T + p_2^R) + \frac{\partial^2 (p_2^T + p_2^R)}{\partial t^2} = 0. \tag{2}$$

An anechoic condition is assumed in the internal cavity, therefore $p_3 = p_3^T$, which satisfies

$$c_3 \nabla^2 p_3^T + \frac{\partial^2 p_3^T}{\partial t^2} = 0. \tag{3}$$

Love's equations, classical thin-shell equations, are used to describe the motions of the two shells [15]. Equations of motion in the axial, radial and circumferential directions of the inner shell are

$$L_1\{u_1^0, v_1^0, w_1^0\} = \rho_i h_i \ddot{u}_1^0, \qquad L_2\{u_1^0, v_1^0, w_1^0\} = \rho_i h_i \ddot{v}_1^0, \tag{4, 5}$$

$$L_3\{u_1^0, v_1^0, w_1^0\} + (p_2^T + p_2^R) - p_3^T = \rho_i h_i \ddot{w}_1^0, \tag{6}$$

where L_1, L_2 and L_3 are differential operators which can be found in reference [15], $\{u_i^0, v_i^0, w_i^0\}$, $i = 1, 2$, represent the displacements of the shell of a point on the neutral surface in the axial, circumferential, radial directions, where the subscripts 1 and 2 denote the variables associated with the inner shell and the outer shell.

For the outer shell, equations of motion in the direction of the axial, radial and circumferential directions are

$$L_1\{u_2^0, v_2^0, w_2^0\} = \rho_e h_e \ddot{u}_2^0, \qquad L_2\{u_2^0, v_2^0, w_2^0\} = \rho_e h_e \ddot{v}_2^0, \tag{7, 8}$$

$$L_3\{u_2^0, v_2^0, w_2^0\} + (p^I + p_1^R) - (p_2^T + P_2^R) = \rho_e h_e \ddot{w}_2^0. \tag{9}$$

At the interfaces between the shells and air, the following equations must be satisfied:

$$\frac{\partial(p^I + p_1^R)}{\partial r} = -\rho_1 \frac{\partial^2 w_2}{\partial t^2} \quad \text{at } r = R_e, \qquad \frac{\partial(p_2^T + p_2^R)}{\partial r} = -\rho_2 \frac{\partial^2 w_2}{\partial t^2} \quad \text{at } r = R_e, \tag{10, 11}$$

$$\frac{\partial(p_2^T + p_2^R)}{\partial r} = -\rho_2 \frac{\partial^2 w_1}{\partial t^2} \quad \text{at } r = R_i, \qquad \frac{\partial p_3^T}{\partial r} = -\rho_3 \frac{\partial^2 w_1}{\partial t^2} \quad \text{at } r = R_i. \tag{12, 13}$$

2.1.2. *Solution procedure*

The solution to equations (1)–(9) that satisfies four boundary conditions in equations (10)–(13) can be obtained using the mode superposition method. The harmonic, plane incident wave p^I can be expressed in the cylindrical co-ordinates as [16]

$$p^I(r, z, \theta, t) = p_0 \sum_{n=0}^{\infty} \varepsilon_n (-\mathrm{j})^n \mathrm{J}_n(k_{1r} r) \cos[n\theta] \mathrm{e}^{\mathrm{j}(\omega t - k_{1z} z)}, \tag{14}$$

where p_0 is the amplitude of the incident wave, n indicates the circumferential mode number, $\varepsilon_n = 1$ for $n = 0$ and 2 for $n = 1, 2, 3 \ldots$, $\mathrm{j} = \sqrt{-1}$, J_n is the Bessel function of the first kind of order n, and ω is the angular frequency. Also, wave numbers in equation (14) are defined as

$$k_1 = \frac{\omega}{c_1}, \quad k_{1z} = k_1 \sin(\gamma_1), \quad k_{1r} = k_1 \cos(\gamma_1), \tag{15}$$

$$k_2 = \frac{\omega}{c_2}, \quad k_{2z} = k_{1z}, \quad k_{2r} = \sqrt{k_2^2 - k_{2z}^2}, \tag{16}$$

$$k_3 = \frac{\omega}{c_3}, \quad k_{3z} = k_{1z}, \quad k_{3r} = \sqrt{k_3^2 - k_{3z}^2}. \tag{17}$$

Owing to the circular cylindrical geometry, the pressures p_1^R, p_2^T, p_2^R and p_3^T are expanded as

$$p_1^R(r, z, \theta, t) = \sum_{n=0}^{\infty} p_{1n}^R H_n^2(k_{1r}r)\cos[n\theta]\mathrm{e}^{\mathrm{j}(\omega t - k_{1z}z)}, \tag{18}$$

$$p_2^T(r, z, \theta, t) = \sum_{n=0}^{\infty} p_{2n}^T H_n^1(k_{2r}r)\cos[n\theta]\mathrm{e}^{\mathrm{j}(\omega t - k_{1z}z)}, \tag{19}$$

$$p_2^R(r, z, \theta, t) = \sum_{n=0}^{\infty} p_{2n}^R H_n^2(k_{2r}r)\cos[n\theta]\mathrm{e}^{\mathrm{j}(\omega t - k_{1z}z)}, \tag{20}$$

$$p_3^T(r, z, \theta, t) = \sum_{n=0}^{\infty} p_{3n}^T H_n^1(k_{3r}r)\cos[n\theta]\mathrm{e}^{\mathrm{j}(\omega t - k_{1z}z)}, \tag{21}$$

where H_n^1 and H_n^2 are Hankel functions of the first and second kinds of order n. Note that the expressions satisfy the wave equations (1)–(3) and the directions of the travelling waves automatically.

Since the trace velocities of all travelling waves have to be the same, shell displacements can be expressed as

$$w_1^0(z, \theta, t) = \sum_{n=0}^{\infty} w_{1n}^0 \cos[n\theta]\mathrm{e}^{\mathrm{j}(\omega t - k_{1z}z)}, \qquad u_1^0(z, \theta, t) = \sum_{n=0}^{\infty} u_{1n}^0 \cos[n\theta]\mathrm{e}^{\mathrm{j}(\omega t - k_{1z}z)}, \tag{22, 23}$$

$$v_1^0(z, \theta, t) = \sum_{n=0}^{\infty} v_{1n}^0 \sin[n\theta]\mathrm{e}^{\mathrm{j}(\omega t - k_{1z}z)}, \qquad w_2^0(z, \theta, t) = \sum_{n=0}^{\infty} w_{2n}^0 \cos[n\theta]\mathrm{e}^{\mathrm{j}(\omega t - k_{1z}z)}, \tag{24, 25}$$

$$u_2^0(z, \theta, t) = \sum_{n=0}^{\infty} u_{2n}^0 \cos[n\theta]\mathrm{e}^{\mathrm{j}(\omega t - k_{1z}z)}, \qquad v_2^0(z, \theta, t) = \sum_{n=0}^{\infty} v_{2n}^0 \sin[n\theta]\mathrm{e}^{\mathrm{j}(\omega t - k_{1z}z)}, \tag{26, 27}$$

Reference [15] explains the choice of the displacement functions for the in-plane displacements u and v in relation to those for w in the cylindrical shell.

Substituting the expressions in equations (18)–(27) in to six shell equations (equations (4)–(9)) and four boundary conditions (equations (10)–(13)) provides 10 equations. These equations can be used to solve for 10 unknowns: p_1^R, p_2^T, p_2^R, p_3^T, u_1^0, v_1^0, w_1^0, u_2^0, v_2^0 and w_2^0 in terms of the amplitude of the incident wave p_0. Six shell vibration equations are

$$u_{1n}^0\left[\rho_i h_i\omega^2 - K_i k_{1z}^2 - \frac{K_i(1-\mu_i)}{2R_i^2}\right] - \frac{K_i(1+\mu_i)}{2R_i} n k_{1z} v_{In}^0 \mathrm{j} - \frac{K_i\mu_i}{R_i} k_{1z} w_{In}^0 \mathrm{j} = 0, \tag{28}$$

$$\begin{aligned} &u_{1n}^0\left[\frac{K_i(1+\mu_i)}{2R_i} k_{1z} n\mathrm{j} + \frac{K_i}{R_i}\mu_i k_{1z} n\mathrm{j} - \frac{D_i}{R_i^2}\mu_i k_{1z}^2 n\right] \\ &\quad + v_{In}^0\left[-\frac{-K_i(1-\mu_i)}{2} k_{1z}^2 - \frac{K_i}{R_i^2} n^2 + \frac{D_i(1-\mu_i)}{R_i^2} k_{1z}^2 + \frac{D_i}{R_i^4} n^2 + \rho_i h_i\omega^2\right] \\ &\quad + w_{In}^0\left[-\frac{K_i}{R_{ii}^2} n - \frac{D_i(1-\mu_i)}{R_i^2} k_{1z}^2 n - \frac{D_i}{R_i^4} n^3\right] = 0, \end{aligned} \tag{29}$$

$$u_{2n}^0\left[-D_i k_{1z}^4-\frac{D_i}{R_i^2}\mu_i k_{1z}^2 n^2+\frac{K_i}{R_i}\mu_i k_{1z}\mathrm{j}\right]+v_{2n}^0\left[\frac{D_i}{R_i^2}\mu_i k_{1z}^2 n+\frac{2D_i(1-\mu_i)}{R_i^2}k_{1z}^2 n^2+\frac{D_i}{R_i^4}n^3-\frac{K_i}{R_i^2}n\right]$$

$$+w_{2n}^0\left[-\frac{D_i\mu_i}{R_i^2}k_{1z}^2 n^2-\frac{2D_i(1-\mu_i)}{R_i^2}k_{1z}^2 n^2-\frac{D_i}{R_i^4}n^4-\frac{K_i}{R_i^2}+\rho_i h_i\omega^2\right]+p_{2n}^T H_n^1(k_{2r}R_i)$$

$$+p_{2n}^R H_n^2(k_{2r}R_i)-p_{3n}^T H_n^1(k_{3r}R_i)=0, \tag{30}$$

$$u_{2n}^0\left[\rho_e h_e\omega^2-K_e k_{1z}^2-\frac{K_e(1-\mu_e)}{2R_e^2}\right]-\frac{K_e(1+\mu_e)}{2R_e}nk_{1z}v_{2n}^0\mathrm{j}-\frac{K_e\mu_e}{R_e}k_{1z}w_{2n}^0\mathrm{j}=0, \tag{31}$$

$$u_{2n}^0\left[\frac{K_e(1-\mu_e)}{2R_e}k_{1z}n\mathrm{j}+\frac{K_e}{R_e}\mu_e k_{1z}n\mathrm{j}-\frac{D_e}{R_e^2}\mu_e k_{1z}^2 n\right]$$

$$+v_{2n}^0\left[-\frac{-K_e(1-\mu_e)}{2}k_{1z}^2-\frac{K_e}{R_e^2}n^2+\frac{D_e(1-\mu_e)}{R_e^2}k_{1z}^2+\frac{D_e}{R_e^4}n^2+\rho_e h_e\omega^2\right]$$

$$+w_{2n}^0\left[-\frac{K_e}{R_e^2}n-\frac{D_e(1-\mu_e)}{R_e^2}k_{1z}^2 n-\frac{D_e}{R_e^4}n^3\right]=0, \tag{32}$$

$$u_{2n}^0\left[-D_e k_{1z}^4-\frac{D_e}{R_e^2}\mu_e k_{1z}^2 n^2+\frac{K_e}{R_e}\mu_e k_{1z}\mathrm{j}\right]+v_{2n}^0\left[\frac{D_e}{R_e^2}\mu_e k_{1z}^2 n+\frac{2D_e(1-\mu_e)}{R_e^2}k_{1z}^2 n^2+\frac{D_e}{R_e^4}n^3-\frac{K_e}{R_e^2}n\right]$$

$$+w_{2n}^0\left[-\frac{D_e\mu_e}{R_e^2}k_{1z}^2 n^2-\frac{2D_e(1-\mu_e)}{R_e^2}k_{1z}^2 n^2-\frac{D_e}{R_e^4}n^4-\frac{K_e}{R_e^2}+\rho_e h_e\omega^2\right]$$

$$+p_{1n}^R H_n^2(k_{1r}R_e)-p_{2n}^T H_n^1(k_{2r}R_e)-p_{2n}^R H_n^2(k_{2r}R_e)=-p_0\varepsilon_n(-\mathrm{j})^n \mathrm{J}_n(k_{1r}R_e). \tag{33}$$

In the above equations, the membrane stiffness and bending stiffness K and D are defined as follows [15]:

$$K_i=\frac{E_i h_i}{1-\mu_i^2}\quad\text{and}\quad K_e=\frac{E_e h_e}{1-\mu_e^2}, \tag{34}$$

$$D_i=\frac{E_i h_i^3}{12(1-\mu_i^2)}\quad\text{and}\quad D_e=\frac{E_e h_e^3}{12(1-\mu_e^2)}. \tag{35}$$

Four equations from the boundary conditions are

$$p_{1n}^R H_n^{2'}(k_{1r}R_e)k_{1r}-\rho_1\omega^2 w_{2n}^0=-p_0\varepsilon_n(-\mathrm{j})^n \mathrm{J}_n'(k_{1r}R_e)k_{1r}, \tag{36}$$

$$p_{2n}^T H_n^{1'}(k_{2r}R_e)k_{2r}+p_{2n}^R H_n^{2'}(k_{2r}R_e)k_{2r}-\rho_2\omega^2 w_{2n}^0=0, \tag{37}$$

$$p_{2n}^T H_n^{1'}(k_{2r}R_i)k_{2r}+p_{2n}^R H_n^{2'}(k_{2r}R_i)k_{2r}-\rho_2\omega^2 w_{1n}^0=0, \tag{38}$$

$$p_{3n}^T H_n^{1'}(k_{3r}R_e)k_{3r}-\rho_3\omega^2 w_{1n}^0=0, \tag{39}$$

where $(\,)'=\mathrm{d}/\mathrm{d}r$.

Equations (28)–(39) constitute 10 equations for 10 unknowns, which can be put into a matrix equation:

$$\begin{bmatrix} 0 & 0 & 0 & 0 & A & B & C & 0 & 0 & 0 \\ 0 & 0 & 0 & 0 & D & E & F & 0 & 0 & 0 \\ G & H & I & 0 & J & K & L & 0 & 0 & 0 \\ 0 & 0 & 0 & 0 & 0 & 0 & 0 & M & N & O \\ 0 & 0 & 0 & 0 & 0 & 0 & 0 & P & Q & R \\ 0 & S & T & U & 0 & 0 & 0 & V & W & X \\ Y & 0 & 0 & 0 & 0 & 0 & Z & 0 & 0 & 0 \\ 0 & A1 & B1 & 0 & 0 & 0 & C1 & 0 & 0 & 0 \\ 0 & D1 & E1 & 0 & 0 & 0 & 0 & 0 & 0 & F1 \\ 0 & 0 & 0 & G1 & 0 & 0 & 0 & 0 & 0 & H1 \end{bmatrix} \begin{Bmatrix} p_{1n}^R \\ p_{2n}^T \\ p_{2n}^R \\ p_{3n}^T \\ u_{2n}^0 \\ v_{2n}^0 \\ w_{2n}^0 \\ u_{1n}^0 \\ v_{1n}^0 \\ w_{1n}^0 \end{Bmatrix} = \begin{Bmatrix} 0 \\ 0 \\ I1 \\ 0 \\ 0 \\ 0 \\ J1 \\ 0 \\ 0 \\ 0 \end{Bmatrix}, \tag{40}$$

where

$$A = \left[\rho_e h_e \omega^2 - K_e k_{1z}^2 - \frac{K_e(1-\mu_e)}{2R_e^2} \right], \quad B = \left[-\frac{K_e(1+\mu_e)}{2R_e} n k_{1z} \mathrm{j} \right], \quad C = -\frac{K_e \mu_e}{R_e} k_{1z} \mathrm{j},$$

$$D = \left[\frac{K_e(1-\mu_e)}{2R_e} k_{1z} n \mathrm{j} + \frac{K_e}{R_e} \mu_e k_{1z} n \mathrm{j} - \frac{D_e}{R_e^2} \mu_e k_{1z}^2 n \right],$$

$$E = \left[-\frac{K_e(1-\mu_e)}{2} k_{1z}^2 - \frac{K_e}{R_e^2} n^2 + \frac{D_e(1-\mu_e)}{R_e^2} k_{1k}^2 + \frac{D_e}{R_e^4} n^2 + \rho_e h_e \omega^2 \right],$$

$$F = \left[-\frac{K_e}{R_e^2} n - \frac{D_e(1-\mu_e)}{R_e^2} k_{1n}^2 n - \frac{D_e}{R_e^4} n^3 \right],$$

$$G = H_n^2(k_{1r} R_e), \quad H = -H_n^1(k_{2r} R_e), \quad I = -H_n^2(k_{2r} R_e),$$

$$J = \left[-D_e k_{1z}^4 - \frac{D_e}{R_e^2} \mu_e k_{1z}^2 n^2 + \frac{K_e}{R_e} \mu_e k_{1z} \mathrm{j} \right],$$

$$K = \left[\frac{D_e}{R_e^2} \mu_e k_{1z}^2 n + \frac{D_e(1-\mu_e)}{R_e^2} k_{1z}^2 n + \frac{D_e}{R_e^4} n^3 - \frac{K_e}{R_e^2} n \right],$$

$$L = \left[-\frac{D_e \mu_e}{R_e^2} k_{1z}^2 n^2 - \frac{2D_e(1-\mu_e)}{R_e^2} k_{1z}^2 n^2 - \frac{D_e}{R_e^4} n^4 - \frac{K_e}{R_e^2} + \rho_e h_e \omega^2 \right],$$

$$M = \left[\rho_i h_i \omega^2 - K_i k_{1z}^2 - \frac{K_i(1-\mu_i)}{2R_i^2} \right],$$

$$N = \left[-\frac{K_i(1+\mu_i)}{2R_i} n k_{1z} \mathrm{j} \right], \qquad O = -\frac{K_i \mu_i}{R_i} k_{1z} \mathrm{j},$$

$$P = \left[\frac{K_i(1-\mu_i)}{2R_i} k_{1z} n\mathrm{j} + \frac{K_i}{R_i} \mu_i k_{1z} n\mathrm{j} - \frac{D_i}{R_i^2} \mu_i k_{1z}^2 n \right],$$

$$Q = \left[-\frac{K_i(1-\mu_i)}{2} k_{1z}^2 - \frac{K_i}{R_i^2} n^2 + \frac{D_i(1-\mu_i)}{R_i^2} k_{1k}^2 + \frac{D_i}{R_i^4} n^2 + \rho_i h_i \omega^2 \right],$$

$$R = \left[-\frac{K_i}{R_i^2} n - \frac{D_i(1-\mu_i)}{R_i^2} k_{1n}^2 n - \frac{D_i}{R_i^4} n^3 \right],$$

$$S = H_n^1(k_{2r} R_i), \quad T = H_n^2(k_{2r} R_i), \quad U = -H_n^1(k_{3r} R_i),$$

$$V = \left[-D_i k_{1z}^4 - \frac{D_i}{R_i^2} \mu_i k_{1z}^2 n^2 + \frac{K_i}{R_i} \mu_i k_{1z} \mathrm{j} \right],$$

$$W = \left[\frac{D_i}{R_i^2} \mu_i k_{1z}^2 n + \frac{D_i(1-\mu_i)}{R_i^2} k_{1z}^2 n + \frac{D_i}{R_i^4} n^3 - \frac{K_i}{R_i^2} n \right],$$

$$X = \left[-\frac{D_i \mu_i}{R_i^2} k_{1z}^2 n^2 - \frac{2D_i(1-\mu_i)}{R_i^2} k_{1z}^2 n^2 - \frac{D_i}{R_i^4} n^4 - \frac{K_i}{R_i^2} + \rho_i h_i \omega^2 \right],$$

$$Y = H_n^{2'}(k_{1r} R_e) k_{1r}, \quad Z = -\rho_1 \omega^2, \quad A1 = H_n^{1'}(k_{2r} R_e) k_{2r}, \quad B1 = H_n^{2'}(k_{2r} R_e) k_{2r},$$

$$C1 = -\rho_2 \omega^2, \quad D1 = H_n^{1'}(k_{2r} R_i) k_{2r}, \quad E1 = H_n^{2'}(k_{2r} R_i) k_{2r},$$

$$F1 = -\rho_2 \omega^2, \quad G1 = H_n^{1'}(k_{3r} R_i) k_{3r}, \quad H1 = -\rho_3 \omega^2,$$

$$I1 = -p_0 \varepsilon_n (-\mathrm{j})^n \mathrm{J}_n(k_{1r} R_e), \quad J1 = -p_0 \varepsilon_n (-\mathrm{j})^n \mathrm{J}_n'(k_{1r} R_e) k_{1r}.$$

The 10 unknown coefficients p_{1n}^R, p_{2n}^T, p_{2n}^R, p_{3n}^T, u_{1n}^0, v_{1n}^0, w_{1n}^0, u_{2n}^0, v_{2n}^0 and w_{2n}^0 are obtained in terms of p_0 by solving equation (40) using Cramer's rule [17]. These can be substituted back into equations (18)–(27) to find the displacements of the shell and the acoustic pressures in series forms.

2.1.3. *Solution in terms of the transmission loss* (TL)

The sound power transmitted to the interior cavity per unit length of the shell is

$$W^T = \sum_{n=0}^{\infty} \frac{1}{2} \mathrm{Re}\{p_{3n}^T \, \partial/\partial t (w_{1n}^0)^*\} \times \int_0^{2\pi} \cos^2 n\theta R_i \, \mathrm{d}\theta$$

$$= \sum_{n=0}^{\infty} \frac{\pi R_i}{2\varepsilon_n} \times \mathrm{Re}\{p_{3n}^T \, \partial/\partial t (w_{1n}^0)^*\}, \tag{41}$$

where $\mathrm{Re}\{\cdot\}$ and the superscript * represent the real part and the complex conjugate of the argument, $\varepsilon_n = 1$ for $n = 0$ and $\varepsilon_n = 2$ for $n = 1, 2, 3, \ldots$. Substitution of equations (21) and

TABLE 1

Parameters to calculate TLs of the double shell at the muffler condition

	Outside air	Outer shell	Air-gap	Inner shell	Inside air
Temperature (°C)	20	—	70	—	103
Density (kg/m^3)	ρ_1 1·21	ρ_e 7750	ρ_2 1·03	ρ_i 7750	ρ_3 0·94
Speed of sound (m/s)	c_1 343	c_e 6100	c_2 371	c_i 6100	c_3 389

(22) for p_3^T and w_1^0 into equation (41) yields an expression for W^T:

$$W^T = \sum_{n=0}^{\infty} \frac{\pi R_i}{2\varepsilon_n} \times \mathrm{Re}\{p_{3n}^T \times H_n^1(k_{3r}R_i)(\mathrm{j}\omega w_{1n}^0)^*\}. \tag{42}$$

TL is defined by

$$TL = -10 \log_{10} \frac{W_n^T}{W^I}, \tag{43}$$

where W^I is the incident power per unit length of the shell in the axial direction

$$W^I = \frac{\cos(\gamma_1)p_0^2}{\rho_1 c_1} \times 2R_0. \tag{44}$$

Thus, an exact expression for TL can be obtained by substituting equations (42) and (44) into equation (43) as follows:

$$TL = -10 \log_{10} \sum_{n=1}^{\infty} \frac{\mathrm{Re}\{p_{3n}^T \times H_n^1(k_{3r}R_i) \times (\mathrm{j}\omega w_{1n}^0)^*\} \times \rho_1 c_1 \pi \times R_i}{4\varepsilon_n R_0 \cos(\gamma_1) p_0^2}. \tag{45}$$

The TL curves of single-walled and double-walled shells calculated in this manner are shown in Figure 3. The geometry of the shells used in the calculation are $R_e = 0{\cdot}1$ m, $R_i = 0{\cdot}09949$ m, $h_e = 0{\cdot}6$ mm, $h_i = 0{\cdot}4$ mm, $h_g = 0{\cdot}01$ mm, for the double-walled shell, and 0·1 m radius and 1 mm thickness for the single-walled shell. The material of the shells is steel, whose Young's modulus and the Poisson ratio are $E = 1{\cdot}9 \times 10^{11}$ Pa, and $\mu = 0{\cdot}3$. The temperature of the interior cavity is taken as 103°C, which is a typical operating condition of the automative muffler. The incident angle of 45° is used for the figures. Parameters used in the calculation to obtain Figure 3 are listed in Table 1 for the double-shell case, from which parameters for the single-shell case can also be obtained by ignoring the parameters corresponding to one of the shells and the air-gap. The condition in Table 1 is referred to as the *muffler condition.*

2.2. SOUND TRANSMISSION ANALYSIS BY PLANE WAVE MODEL

In this case, the problem is idealized as a 1-D wave propagation problem as shown in Figure 2.

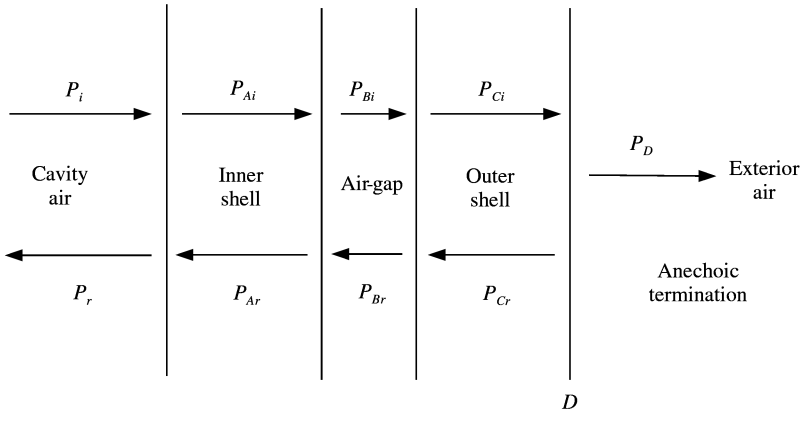

Figure 2. Schematic description of the problem: 1-D model.

The four-pole method can be used conveniently for this type of analysis [18]. The four-pole equation between the system's input and output variables are

$$\begin{Bmatrix} p_A \\ v_A \end{Bmatrix} = \begin{bmatrix} \cos k_A l_A & \mathrm{j} r_A \sin k_A l_A \\ \dfrac{\mathrm{j}}{r_A} \sin k_A l_A & \cos k_A l_A \end{bmatrix} \begin{bmatrix} \cos k_B l_B & \mathrm{j} r_B \sin k_B l_B \\ \dfrac{\mathrm{j}}{r_B} \sin k_B l_B & \cos k_B l_B \end{bmatrix} \begin{bmatrix} \cos k_C l_C & \mathrm{j} r_C \sin k_C l_C \\ \dfrac{\mathrm{j}}{r_C} \sin k_C l_C & \cos k_C l_C \end{bmatrix} \begin{Bmatrix} p_D \\ v_D \end{Bmatrix}, \tag{46}$$

where p and v are the acoustic pressure and particle velocities, k, r and l indicate the complex wave number, characteristic impedance, the thickness of each layer respectively. Subscripts A, B and C refer parameters corresponding to the outer shell, the air-gap and the inner shell respectively. On multiplying matrices in equation (46), the system equation is contained as

$$\begin{Bmatrix} p_A \\ v_A \end{Bmatrix} = \begin{bmatrix} A_{11} & A_{12} \\ A_{21} & A_{22} \end{bmatrix} \begin{Bmatrix} 1 \\ \dfrac{1}{r_D} \end{Bmatrix} p_D. \tag{47}$$

Since the total particle velocity and pressure v_A and p_A can be expressed as

$$v_A = v_i - v_r = \frac{p_i - p_r}{r_A} = \left(\frac{A_{21}}{r_D} + A_{22} \right) p_D, \tag{48}$$

therefore

$$p_i - p_r = r_A v_A = r_A \left(\frac{A_{21}}{r_D} + A_{22} \right) p_D. \tag{49}$$

Also

$$p_A = p_i + p_r = \left(\frac{A_{11}}{r_D} + A_{12} \right) p_D. \tag{50}$$

From equations (49) and (50), the incident pressure p_i and the reflective pressure p_r can be separated, and the reflection coefficient R can be obtained as

$$R = \frac{p_r}{p_i} = \frac{A_{11}/r_D + A_{12} - r_A/r_D\, A_{22} - r_A A_{22}}{A_{11}/r_D + A_{12} + r_A/r_D\, A_{22} + r_A A_{22}}. \tag{51}$$

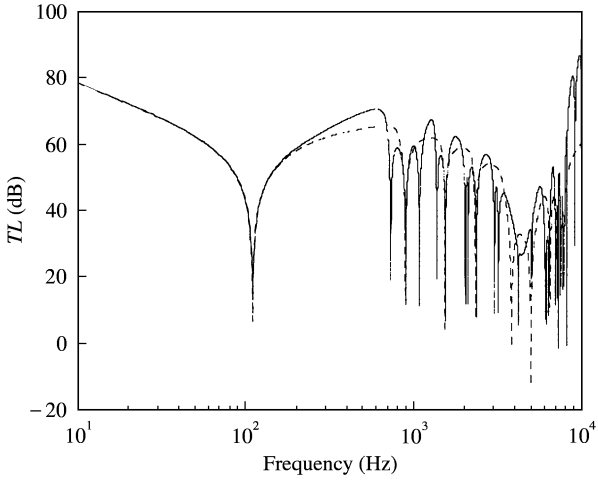

Figure 3. TLs calculated from 2-D model at muffler condition: - - - - -, single shell ($R = 0{\cdot}1$ m, $h = 1{\cdot}0$ mm); ——, double shell ($R_e \cong R_i = 0{\cdot}1$ m, $h_i = 0{\cdot}6$ mm, $h_0 = 0{\cdot}4$ mm).

Since the cross-sectional area of the input and output side of the system are the same in this case, the power transmission coefficient becomes

$$T_\pi = 1 - |R|^2. \tag{52}$$

Finally, the transmission loss can be estimated from the power transmission coefficient:

$$TL(\mathrm{d}B) = 10 \log_{10} \frac{1}{T_\pi}. \tag{53}$$

The TL curves calculated by this 1-D model are shown in Figure 4 for the same system at the same condition used to obtain Figure 3.

2.3. COMBINED SOLUTIONS

The TL curves in Figures 3 and 4 can be combined to represent the system response in the entire frequency range. Considering that lower TL means higher transmitted noise, the rule to combine two TL curves should be picking up the lower TL at each frequency. Figure 5 shows the TL curves of the single shell and the double shell obtained by combining the curves in Figures 3 and 4. These combined TLs are used for comparisons of the the analytical results and the experimental results.

3. COMPARISON WITH EXPERIMENTAL RESULTS

3.1. MEASUREMENT SET-UP

Figure 6 shows the experimental set-up to measure TLs of the shells in an anechoic chamber. The single shell is shown, which has the same appearance as the double shell. A pair of microphones shown in the figure is used to measure the sound intensity on the

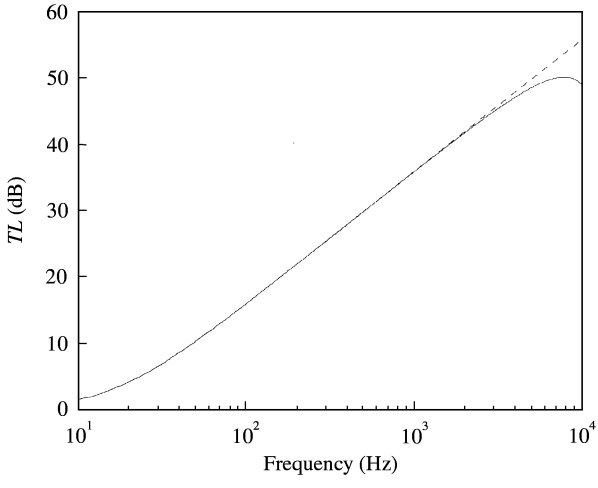

Figure 4. TLs calculated from 1-D model at muffler condition: - - - - -, single shell ($h = 1{\cdot}0$ mm); ——, double shell ($h_i = 0{\cdot}6$ mm, $h_0 = 0{\cdot}4$ mm).

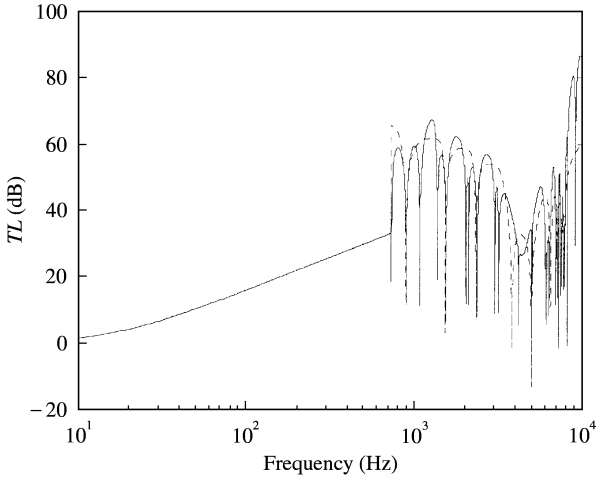

Figure 5. Combined TLs from Figures 3 and 4: - - - - -, single shell; ——, double shell.

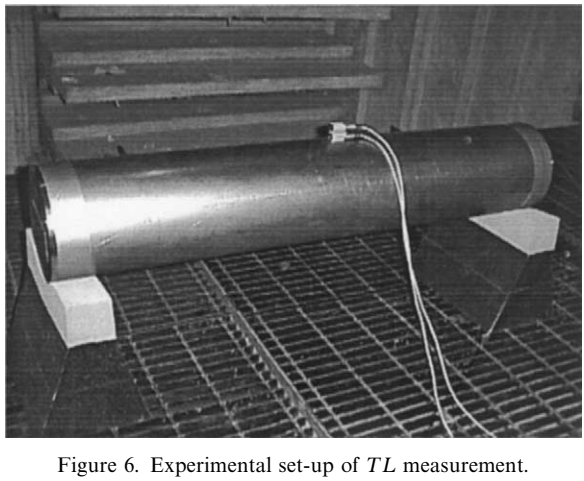

Figure 6. Experimental set-up of TL measurement.

TABLE 2

Parameters to calculate TLs of the double shell at the test condition

	Outside air	Outer shell	Air-gap	Inner shell	Inside air
Temperature (°C)	20	—	20	—	20
Density (kg/m^3)	ρ_1 1·21	ρ_e 7750	ρ_2 1·21	ρ_i 7750	ρ_3 1·21
Speed of sound (m/s)	c_1 343	c_e 6100	c_2 343	c_i 6100	c_3 343

external surface. One more pair of microphones is located at the same position on the internal surface of the shell to measure the sound intensity on the internal surface.

The geometry of the shells used in the experiment is that, with reference to Figure 1, $R_e = 0{\cdot}1$ m, $R_i = 0{\cdot}09$ m, $h_e = 1$ mm, $h_i = 1$ mm, $h_g = 1$ mm, for the doubles shell, and 0·1 m radius and 1 mm thickness for the single-walled shell. The shells were made of steel, which has the Young's modulus $E = 1{\cdot}9 \times 10^{11}$ Pa and the Poisson ratio $\mu = 0{\cdot}3$. The temperature was 20°C throughout the entire system during the measurements. The parameters corresponding to this condition are listed in Table 2 for the double-shell case, from which parameters for the single shell can be easily obtained. The condition defined by Table 2 is referred to as the *test condition*. Obviously, the parameters at the test condition were as used in the simulations that were compared to the measurements in Figures 7(a–c) and 8(a–c).

For both shells, the measurement was conducted once using an internal sound source, and the other time using an external source. The internal source was a 3-in speaker and the external source was a B&K (Type 4296) decahedral speaker. A white noise with the maximum frequency of 6400 Hz was used to drive the sound sources. The frequency resolution of the measurement was 16 Hz.

The internal sound source set-up represents the theoretical model better because it has an anechoic condition externally and reverberant condition internally. This set-up is a rough reciprocal of the theoretical model. The external sound source set-up has incident as well as reflected waves both internally and externally.

3.2. SINGLE SHELL MEASUREMENT

The analytical solutions of the sound transmission through the single shell can be obtained by ignoring the equations corresponding to one of the shells and the annular space. Figures 7(a, b) compare the measured and calculated TLs of the single shell. The calculation was carried out using the *test condition* (see Table 2 for parameters). The incident angle of 70° was used in the calculation, which was estimated based on the relative location between the sound source and the intensity probes. Figure 7(a) is the comparison of the calculation and the test with the source inside and Figure 7(b) is the comparison of the calculation and the test with the source outside.

The figures show that the calculated TL curves agree reasonably with the measured TL curves if the differences between the experimental and theoretical models are considered. It is believed that the measured TL in Figure 7(a) has weaker frequency components in the low frequency range as compared to that in Figure 7(b) because of the limitation of the performance of the 3-in speaker used for the former. On the other hand, the former has stronger frequency components than the latter in the high frequency range, which is

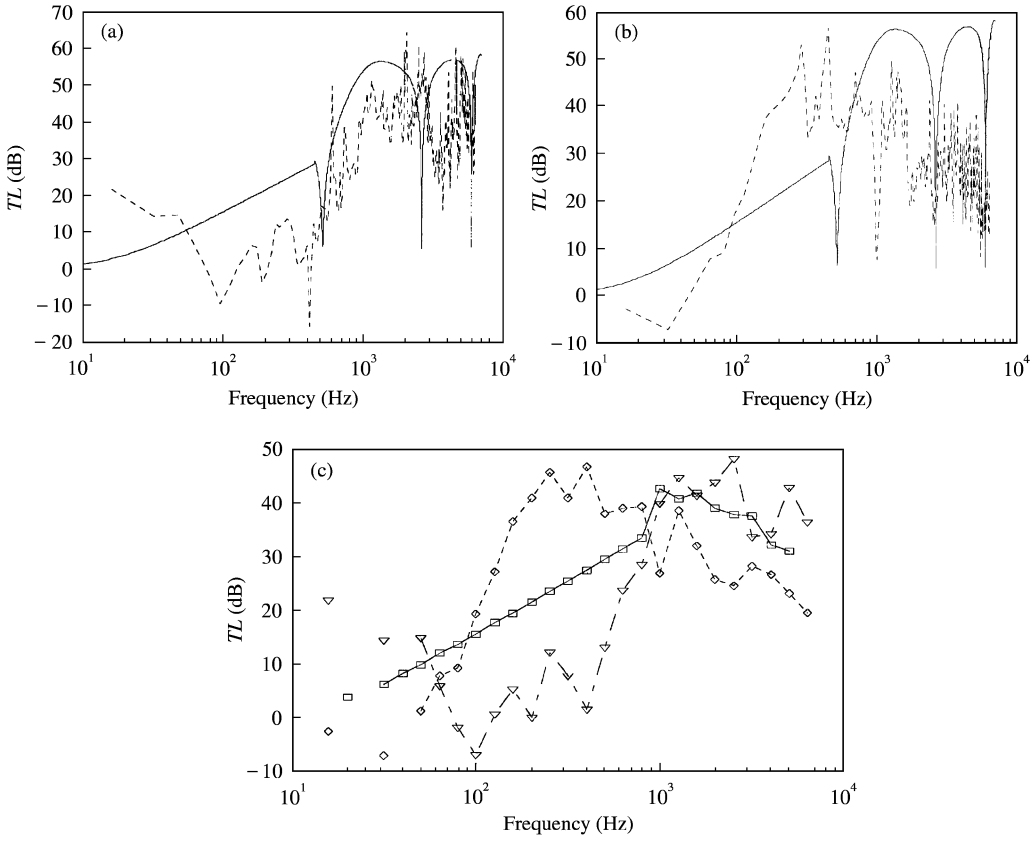

Figure 7. Calculated TL compared with measured TL. (a) Single shell, inside source, ——, calculated; - - - - -, measured. (b) Single shell, outside source, ——, calculated; - - - - -, measured. (c) Single shell, TL averaged for random incident angles (line legends).

believed to be the effect of the stronger direct field of the internal source set-up used in the former. The analytical TL curve generally falls between the two measured TL curves.

The calculated TL obviously depends on the choice of the incident angle in the analysis. This dependency can be removed by averaging TL over all possible incident angles. According to the Paris formula [19, 20], the average power transmission coefficient $\bar{\tau}$ is given as

$$\bar{\tau} = 2 \int_0^{\theta_m} \tau(\theta) \sin\theta \cos\theta \, \mathrm{d}\theta, \tag{54}$$

where $\tau(\theta)$ is the power transmission coefficient calculated for the incident angle θ, and θ_m is the maximum incident angle, which is chosen as 80° according to the suggestion by Mulholland *et al.* [9]. Then, the average TL is obtained as

$$TL_{avg} = 10 \log \frac{1}{\bar{\tau}}. \tag{55}$$

The integration in equation (54) is conducted numerically by Simpson's rule using an integration step-size of 2°. Figure 7(c) compares TL_{avg} to the two measured TLs in a third

octave format, which shows that the TL_{avg} lies between the two measured TL curves. Bigger differences between the curves in the low-frequency range may be attributed to the effect of the boundary condition, a major difference between the experimental and theoretical models, which becomes more significant in low-frequency modes.

3.3. DOUBLE SHELL MEASUREMENT

Figures 8(a, b) show comparisons between the calculated and measured TL curves of the double-walled shell. Trends similar to the single-shell case are found in the double-shell case. Figure 8(c) compares to two measured TL curves and TL_{avg} curve using a third octave band format for the double-walled shell.

4. PARAMETER STUDIES

Effects of design parameters and system parameters are studied analytically in terms of their effects on the TL. The simulations for the parameter studies are made at the *muffler condition* (see Table 1).

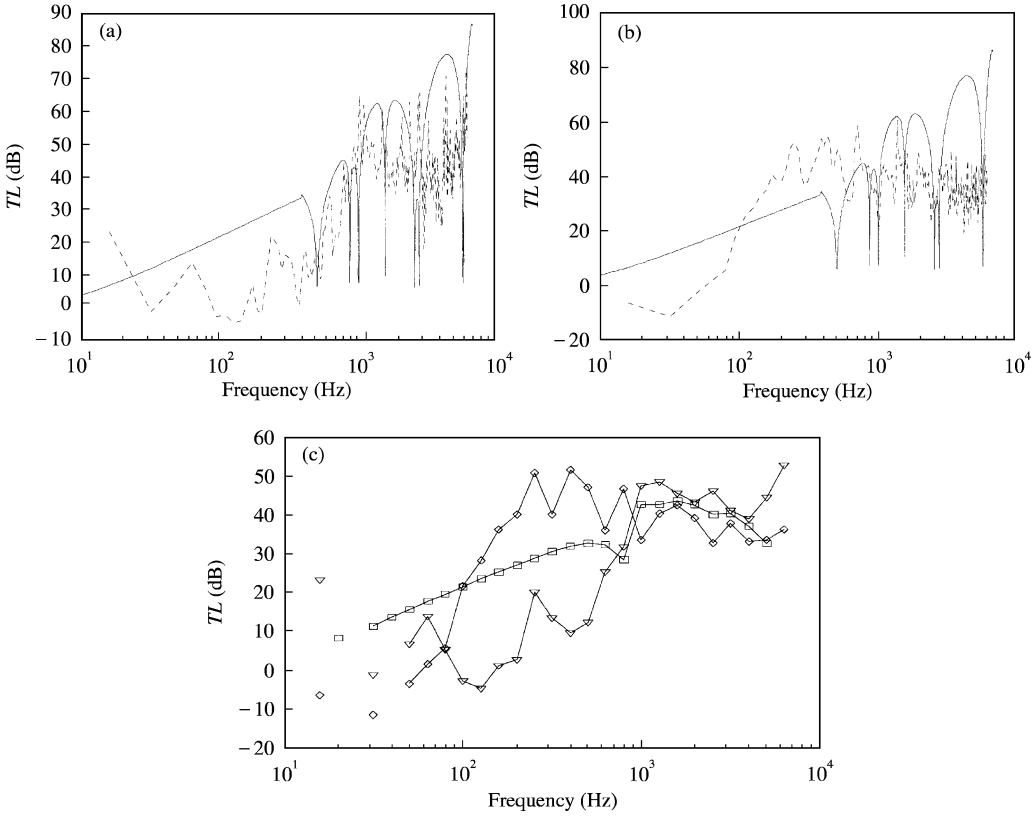

Figure 8. (a) Calculated TL compared with measured TL using inside source, double shell ($R_e \cong R_i = 0{\cdot}1$ m, $h_i = h_0 = 1{\cdot}0$ mm): ——, calculated; - - - - -, measured. (b) Calculated TL compared with measured TL using outside source, double shell ($R_e \cong R_i = 0{\cdot}1$ m, $h_i = h_0 = 1{\cdot}0$ mm): ——, calculated; - - - - -, measured. (c) Averaged TLs compared with measured TLs, double shell.

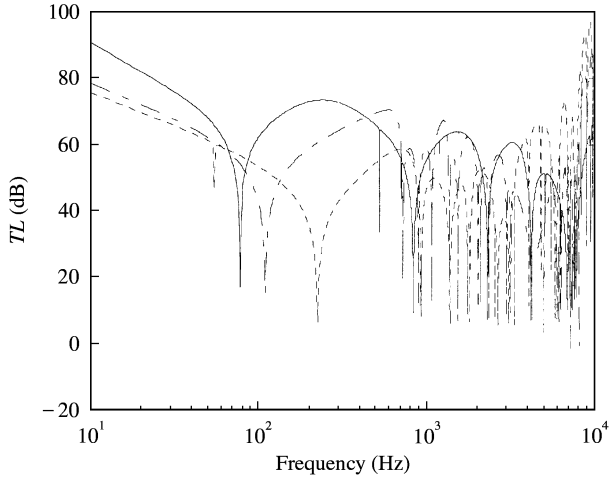

Figure 9. Effect of the incidence angle in TLs of the double shell ($R_e \cong R_i = 0{\cdot}1$ m, $h_i = 0{\cdot}6$ mm, $h_0 = 0{\cdot}4$ mm): - - - - -, 30°; – · – · –, 40°; ——, 60°.

4.1. CHOICE OF INCIDENT ANGLE IN ANALYSIS

The averaging process in equation (54) is very time consuming, which becomes a problem in design iterations, in which the TLs have to be calculated numerous times. Therefore, the effect of the choice of the incident angle is studied to see if the calculation using only one angle can be used for relative comparison purposes. Figure 9 compares the TLs obtained for the incident angles of 30, 45 and 60°. Notice that the TLs in parameter studies shown in Figures 9, 10 and 11 were obtained using only the 2-D model. It is known that the general trend of the TL curves remains the same, although the curves become different as different incident angles are used. Therefore, the incident angle of 45° is chosen for parameter studies later in this work.

4.2. EFFECT OF THE DOUBLE-WALL CONSTRUCTION

Figures 3 and 5 compare the TLs of the single shell of 1 mm thickness and the double shell composed of 0·6 mm walls 0·4 mm apart by a very air-gap (0·01 mm). Since the total thickness of the shells is the same, the comparison shows the effect of the double shell design. From Figures 3 and 5, it is known that the double-wall structure does not help in increasing the TL in the frequency range lower than the coincidence frequency (about 5500 Hz in this case). It will be shown later that the double-wall construction provides better noise insulation as the air-gap size increases, therefore a double-wall construction with large air-gap has an advantage as an acoustic barrier. A large air-gap design in mufflers is not available because the double-wall is made by spot welding, which leaves a very small air-gap. Figure 10 compares the TLs of the single shell of 1 mm thickness and the double shell of two 1 mm walls. In this case, the double shell provides better sound insulation, however, at the cost of doubling the weight.

Based on this study, it is believed that the perceived advantage of the double shell muffler over the single shell counterpart stems not from the better sound isolation characteristics but from the increased damping effect of the double shell.

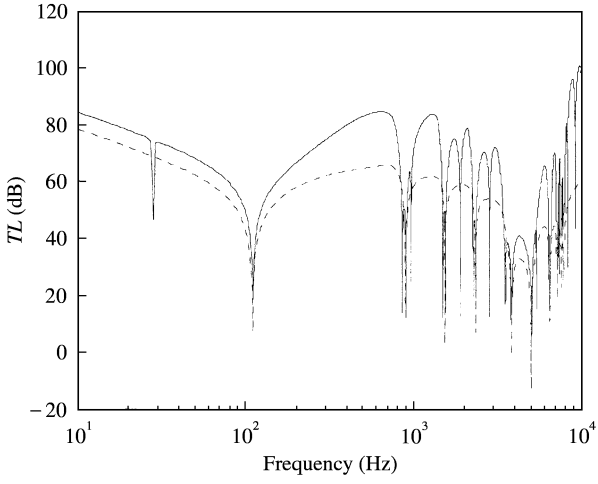

Figure 10. TLs of the single shell ($R = 0{\cdot}1$ m, $h = 1{\cdot}0$ mm) and double ($R_e \cong R_i = 0{\cdot}1$ m, $h_i = h_0 = 1{\cdot}0$ mm): - - - - -, single shell; ——, double shell.

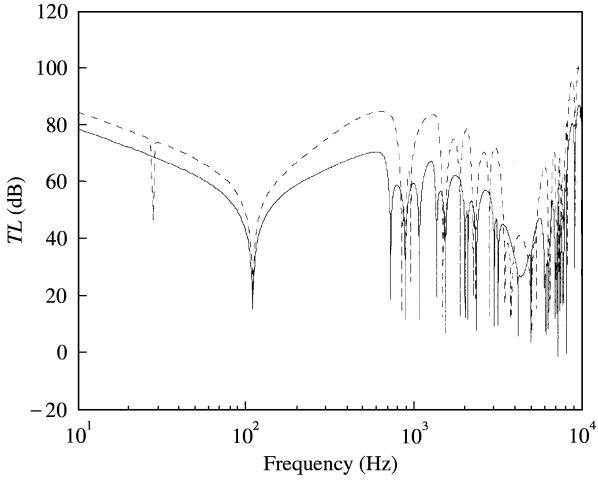

Figure 11. TLs of the double shell ($R_e \cong R_i = 0{\cdot}1$ m) with respect to thickness combination: - - - - -, double shell ($h_i = 1{\cdot}0$ mm, $h_0 = 1{\cdot}0$ mm); ——, double shell ($h_i = 0{\cdot}6$ mm, $h_0 = 0{\cdot}4$ mm).

4.3. EFFECT OF THICKNESS

Figure 11 compares the TLs calculated by the bending wave model for the shell composed of two 1 mm walls and the shell composed of 0·4 and 0·6 mm walls. It is known that the effect of the thickness increase is over a broad range of the frequency.

4.4. EFFECT OF THE AIR-GAP

Figure 12 compares the transmission losses calculated from the bending model for the double shells of different air-gap sizes. Sound transmission through the double shells of 0·6 and 0·4 mm with three air-gap sizes of 0·01, 1 and 10 mm are considered. The figure shows

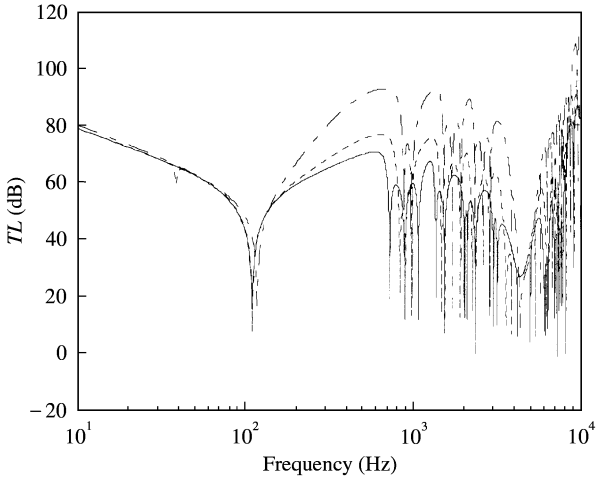

Figure 12. Effect of air-gap in TLs of the double shell ($R_e \cong R_i = 0{\cdot}1$ m, $h_i = 0{\cdot}6$ mm, $h_0 = 0{\cdot}4$ mm): ——, $t_g = 0{\cdot}01$ mm; ------, $t_g = 1{\cdot}0$ mm; – · – · –, $t_g = 10$ mm.

that the transmission loss can be increased quite significantly by enlarging the air-gap size, which is not a possible option for mufflers.

The first two dips in the TL curves in Figure 12 are noteworthy. It is believed that the first dip at around 100 Hz is caused by the lowest overall system natural frequency. The second dip observed at around 770 Hz in Figure 12 corresponds to the first ring frequency of the annular air-gap. This frequency can be estimated as

$$f_{cavity} = \frac{(c_{cavity}/\cos(\gamma_1))}{2\pi R_0} = \frac{c_{phase-speed}}{2\pi R_0}, \tag{56}$$

where c_{cavity} is the sound speed in the cavity, γ_1 is the incidence angle, R_0 is the radius of the shell and $c_{phase-speed}$ stands for the phase speed in the circumferential direction. The frequency is calculated to be approximately 770 Hz at the muffler operating condition.

5. CONCLUSION

An exact solution procedure is developed to study the sound transmission through a double-walled cylindrical shell. The solutions obtained from two models, the first of which describes the sound transmission caused by the bending waves travelling in the shell and the second describes the sound transmission by the plane waves travelling across the layers of two shells and the air-gap. For the bending wave solution, three acoustic wave equations and two shell vibration equations are solved simultaneously, which provides a series solution. This is considered to be the first exact solution to this type of a problem obtained using the full shell vibration equations. To solve the plane wave model, the four-pole method is used. Both solutions are represented in terms of the transmission loss (TL), which are then combined into a single TL curve. Also, the idea of combining the solutions is used for the first time in this work. The analytical solutions obtained are compared with the measured TLs, which show reasonable agreement. The effects of important design parameters such as the air-gap size and the thickness ratio are also studied using the analytical solutions.

REFERENCES

1. Y. Y. TANG, J. H. ROBINSON and R. J. SILCOX 1996 34th AIAA *Aerospace Science Meeting and Exhibit* (*AIAA*-96-0877), 1–10. Sound transmission through a cylindrical sandwich shell with honeycomb core.
2. Y. Y. TANG, R. J. SILCOX and J. H. ROBINSON 1996 *Proceedings of* 14*th International Modal Analysis Conference*, *Detroit*, *MI*, 1488–1492. Sound transmission through two concentric cylindrical sandwich shells.
3. L. L. BERANEK 1949 *Journal of Acoustical Society of America* **21**, 419–428. Sound transmission through multiple structures containing flexible blankets.
4. L. L. BERANEK 1988 *Noise and Vibration*. New York: McGraw-Hill.
5. C.-Y. WANG and R. VAICAITIS 1998 *Journal of Sound and Vibration* **216**, 865–888. Active control of vibrations and noise of double wall cylindrical shells.
6. C. L. DYM and M. A. LANG 1974 *Journal of Acoustical Society of America* **56**, 1523–1532. Transmission of sound through sandwich panels.
7. F. P. GROOTEMAN, D. BOER and H. SCHIPPERS 1995 *CEAA/AIAA* 1*st Joint Aeroacoustic Conference*, *Munich*, *Germany* 1049–1053. Vibro-acoustic analysis of double wall structures.
8. J. PAN, S. J. ELLIOTT and K.-H. BAEK 1999 *Journal of Sound and Vibration* **223**, 543–566. Analysis of low frequency acoustic response in a damped rectangular enclosure.
9. K. A. MULHOLLAND, K. D. PARBROOK and A. CUMMINGS 1967 *Journal of Sound and Vibration* **6**, 324–334. The transmission loss of double panels.
10. A. LONDON 1950 *Journal of Acoustical Society of America* **22**, 270–279. Transmission of reverberate sound through double walls.
11. P. H. WHITE and A. POWELL 1996 *Journal of Acoustical Society of America* **44**, 821–832. Transmission of random sound and vibration through a rectangular double wall.
12. P. WHITE 1996 *Journal of Acoustical Society of America* **40**, 1124–1130. Sound transmission through an infinite, closed, cylindrical shell.
13. J. H. LEE and J. KIM 2000 *Proceedings of International Compressor Conference at Purdue University*, *West Lafayette*, *IN*, 933–940. Sound transmission through cylindrical shell of hermetic compressors. *Journal of Sound and Vibration*. Exact calculation of the transmission loss of the thin shell enclosing cylindrical cavity (under review).
14. L. E. KINSLER, A. R. FREY, A. B. COPPENS and J. V. SANDERS 1982 *Fundamentals of Acoustics*. New York: John Wiley & Sons, Inc.
15. W. SOEDEL 1993 *Vibrations of Shells and Plates*. New York: Marcel Dekker, Inc.
16. M. MORSE and K. U. INGARD 1968 *Theoretical Acoustics*. New York: McGraw-Hill.
17. E. KREYSZIG 1993 *Advanced Engineering Mathematics*. New York: John Wiley & Sons, Inc.
18. M. L. MUNJAL 1987 *Acoustics of Ducts and Mufflers*. New York: Wiley-Interscience.
19. A. D. PIERCE 1981 *Acoustics*. New York: McGraw-Hill.
20. J. S. BOLTON, N. M. SHAU and Y. J. KANG 1996 *Journal of Sound and Vibration* **191**, 317–347. Sound transmission through multi-panel structures lined with elastic porous materials.